PCCP

COMMUNICATION

View Article Online
View Journal | View Issue

Published on 26 January 2016. Downloaded by University of Tennessee at Knoxville on 18/08/2016 18:57:32.

Cite this: *Phys. Chem. Chem. Phys.*, 2016, **18**, 6394

Received 18th November 2015,
Accepted 24th January 2016

DOI: 10.1039/c5cp07088k

www.rsc.org/pccp

# Enhanced sampling simulation analysis of the structure of lignin in the THF–water miscibility gap†‡

Micholas Dean Smith,[abc] Loukas Petridis,[ac] Xiaolin Cheng,[ac] Barmak Mostofian[acd] and Jeremy C. Smith*[abc]

**Using temperature replica-exchange molecular dynamics, we characterize a globule-to-coil transition for a softwood-like lignin biopolymer in a tetrahydrofuran (THF)–water cosolvent system at temperatures at which the cosolvent undergoes a de-mixing transition. The lignin is found to be in a coil state, similar to that in the high-temperature miscible region. Analysis of the transition kinetics indicates that THF acts in a surfactant-like fashion. The present study thus suggests that THF–water based pretreatments may efficiently remove lignin from biomass even at relatively low (non-water boiling) temperatures.**

Cellulosic ethanol, a biofuel derived from lignocellulosic biomass, is a promising alternative to current feedstock (corn ethanol) biofuels.[1] A challenge to adopting lignocellulosic biomass as a sustainable bioenergy source, however, is its recalcitrance to chemical and enzymatic breakdown for the production of fuel precursors.[2] As lignin, a hydrophobic plant polymer, is considered to be a major physical impediment for the conversion of biomass to biofuels, it is particularly important to enhance lignin removal from cellulose fibres.

Tetrahydrofuran (THF) is commonly employed to solubilize lignin[3–5] for its characterization. Recently, a cosolvent-enhanced lignocellulose fractionation (CELF) pre-treatment method has been shown to readily increase biofuel precursor yields. In this pre-treatment, lignocellulosic biomass is immersed in a THF–water cosolvent system and heated to temperatures in excess of 445 K. The efficiency of CELF is attributed to promoting lignin removal from cellulose fibres.[6–9]

Understanding the mechanism behind lignin transformations in THF–water cosolvent will provide fundamental information that may help engineer more efficient biomass pre-treatment methods. Interestingly, during the heating phase of CELF, the cosolvent system passes through a temperature regime where the two solvent species, water and THF, become immiscible, as seen by a transition from a transparent medium to a "cloudy" (opaque) solution.[10,11] At mass ratios of THF-to-water typically used in CELF, the immiscible temperature regime begins near 348 K and ends at temperatures near 410 K.[10,11]

In a previous study[12] we examined the conformations of a softwood-like lignin at four different temperatures and two different THF::water mass ratios using molecular dynamics (MD) simulation and found that, when immersed in an aqueous THF cosolvent environment, lignin no longer adopts the collapsed globular state found in pure water solutions, but instead is a random coil, and is preferentially solvated by THF. This is important because in the coil conformation lignin should not self-aggregate as polymer–solvent interactions would then be preferred over polymer–polymer interactions, making it energetically unfavourable to aggregate, making it more easily removed during CELF pre-treatment. However, in our previous work, we were unable to sufficiently sample the solvent mixtures at temperatures near the immiscible region (a regime that may be interesting for low-temperature pre-treatment) using traditional MD methods. Here, we resolve this issue by using replica exchange MD (REMD) simulations[13–15] to characterize the structure of lignin within the solvent immiscible region.

[a] *Center for Molecular Biophysics, University of Tennessee/Oak Ridge National Laboratory, Oak Ridge, TN, 37830, USA. E-mail: smithjc@ornl.gov; Tel: 1-865-574-9635/591-4805*

[b] *Department of Biochemistry and Cellular and Molecular Biology, University of Tennessee, M407 Walters Life Sciences, 1414 Cumberland Avenue, Knoxville, TN 37996, USA*

[c] *BioEnergy Science Center, Oak Ridge National Laboratory, Oak Ridge, TN 37830, USA*

[d] *Joint Institute for Biological Sciences, University of Tennessee/Oak Ridge National Laboratory, Oak Ridge, TN, 37830, USA*

† This manuscript has been authored by UT-Battelle, LLC under Contract No. DE-AC05-00OR22725 with the U.S. Department of Energy. The United States Government retains and the publisher, by accepting the article for publication, acknowledges that the United States Government retains a non-exclusive, paid-up, irrevocable, world-wide license to publish or reproduce the published form of this manuscript, or allow others to do so, for United States Government purposes. The Department of Energy will provide public access to these results of federally sponsored research in accordance with the DOE Public Access Plan (http://energy.gov/downloads/doe-public-access-plan).

‡ Electronic supplementary information (ESI) available: Additional details regarding the replica-exchange simulation, example kinetic fits, and SASA measurements are provided. See DOI: 10.1039/c5cp07088k



This journal is © the Owner Societies 2016

Published on 26 January 2016. Downloaded by University of Tennessee at Knoxville on 18/08/2016 18:57:32.

REMD improves the conformational sampling in the MD simulations and is well suited for modelling pre-treatment as it enhances the sampling in all simulated temperatures. Further, with the enhanced conformational sampling through REMD we are able to quantify the relaxation kinetics of lignin from a globule to a coil when exposed to the THF–water environment.

Probing the behaviour of lignin within the miscibility gap region is particularly important as it is not conclusively known if the structure of lignin is different compared to those from our previous work in the miscible regimes. Small or no deviations would suggest that the CELF pre-treatment may be performed at lower temperatures and pressures (with the proper catalysts for cellulose degradation) and would thus further reduce the cost of this pre-treatment method for biofuel production.

The molecular model of lignin used is of a linear 61 monomer softwood lignin (Guacyl monomer units only, with varied linkages) modelled initially in a collapsed globular state taken from previous simulations in pure water.[16,17] The interaction potentials for the simulations were the CHARMM force-field for lignin[18] and the CHARMM32[19] ether force-field for THF and the TIP3P[20] water model. Fig. 1 provides a sample lignin structure generated during the simulation.

Simulations were carried out in a three step process of: (1) initial solvation and energy minimization, (2) solvent relaxation obtained by applying positional restraints on all lignin atoms while the solvent relaxes, then removing these restraints and running a short simulation to relax the system to the target pressure (1 bar), and (3) production run in an NPT ensemble. The lignin structure was then solvated in a 0.4 THF :: water mass-ratio co-solvent solution in a periodic box with an initial volume of $\sim$2340 nm$^3$ (203 597 atoms: 47 680 water molecules, 4536 THF molecules, and 1 lignin polymer). Energy minimization was performed for a maximum of 10 000 steps, with a tolerance of 100 kJ (mol nm)$^{-1}$. Solvent relaxation (MD) was performed with the positions of lignin atoms fixed and the system pressure was set to 1 bar for each temperature window. The temperature and pressure were kept constant with the Berendsen thermo/barostat.[21] For the production/replica-exchange simulation the V-Rescale[22] thermostat and Parrinello–Rahman[23] barostat were used.

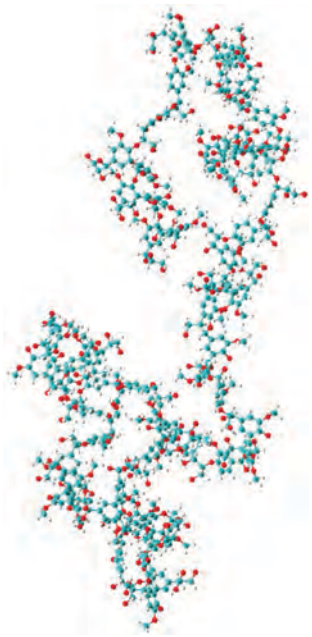

Fig. 1 Sample lignin structure.

Our use of a single chain (*i.e.* infinite dilution conditions) in probing the lignin–cosolvent interactions can be justified by noting that there is a direct correspondence between the presence/absence of the coil state and the aggregation/disaggregation of polymers; the coil state is only present when the (co)solvent–lignin interaction is preferable to the lignin–lignin self-interaction and no aggregation is observed. In contrary, when lignin self-interactions dominate this would lead to lignin aggregation in the presence of multiple lignin molecules or, equivalently, a globule under dilute conditions.

In order to enhance the sampling of the system near the solvent phase separation temperature regime (near 348 K for the mass fraction used in the simulation), we used 125 replicas with temperatures from 305 K to 364 K. The massive number of replicas are necessary to allow for exchanges to occur across the solvent phase separation-boundary. In both the solvent relaxation and replica-exchange simulations a timestep of 2 fs was used, with a frame-saving rate of 10 ps. Additionally, in the production and relaxation simulations all bonds distances were fixed with the LINCS[24,25] and SETTLE[26] algorithms. In the production run, exchanges between replicas were attempted every 500 steps, with an average exchange probability of $\sim$0.5. Production runs were performed for a total of 125 ns per replica. All simulations were performed using the GROMACS 5.0.2 simulation suite[27–31] on the TITAN supercomputer, using $\sim$144 000 cores of the machine (nearly half of the entire supercomputer's resources), at the Oak Ridge Leadership Computing Facility.

In order to measure changes to lignin structure near the onset of the cosolvent immiscibility, we calculated the mass-fractal dimension ($\alpha$), the solvent accessible surface area, lignin–lignin hydrogen bonds (with an angle cutoff of 30° and a distance cutoff of 0.35 nm between donors and acceptors), the radius of gyration ($R_g$), and radial distribution functions of lignin. The mass-fractal dimension ($\alpha$), used to classify the globule and coil states, was obtained by fitting a power law to the radius of gyration of the polymer as a function of the number of monomers ($N$) in the chain, $R_g \sim N^{\nu}$, and converting the scaling exponent ($\nu$) into a fractal dimension ($\alpha$). The typical conversion between scaling exponent and the fractal dimension is a simple reciprocal; however, as lignin is a hydrophobic polymer, and for ease of comparison with our previous work,[12] we instead make use of the relation $\nu = (\alpha + 2)(5\alpha)^{-1}$ as this was specifically derived for hydrophobic chains.[32] This mass-fractal dimension was computed using the VMD software suite.[33]

The probability distribution of fractal dimension, 2D-histograms as function of the radius of gyration and the number of lignin–lignin hydrogen bonds, and hydrophobic solvent accessible surface area (SASA) are presented at six different temperatures in Fig. 2, 3 and ESI‡ Fig. S1. Regardless of temperature

Published on 26 January 2016. Downloaded by University of Tennessee at Knoxville on 18/08/2016 18:57:32.

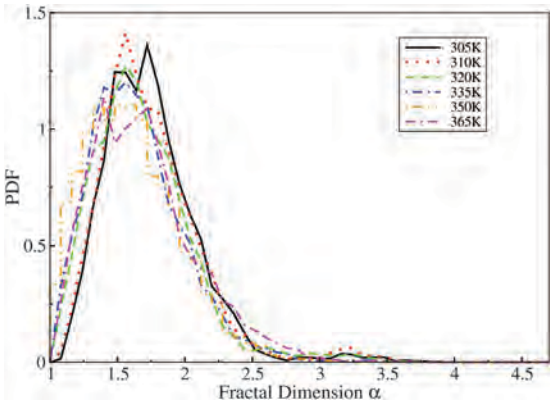


Fig. 2 Distribution of fractal dimension (α) at six different temperatures. Constructed by using the last 75 ns of the noted temperature-replicas. $\alpha < 2.5$ indicate coil states and make up ~94% to 96.5% of all states sampled.

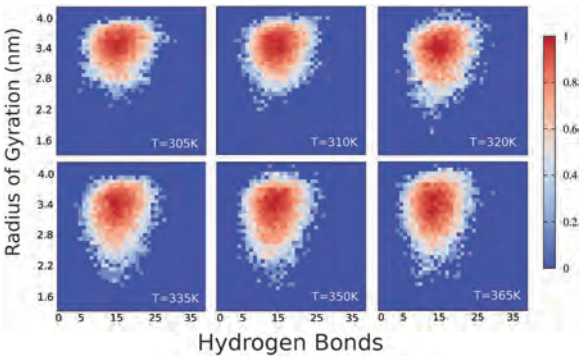


Fig. 3 2D-Histograms of the radius of gyration and the number of intra-lignin hydrogen-bonds (a hydrogen bond is considered to be formed if the donor–acceptor distance is less than 0.3 nm and the donor–hydrogen–acceptor angle less than 20°). The natural-logarithm of the normalized counts is proportional to free-energy.

(and thus co-solvent immiscibility) there is only a single dominant structural state for lignin. Closer examination reveals that at temperatures higher than 310 K, α primarily adopts values associated with a random-coil ($\alpha < 2.5$), along with a very small fraction of globule states (the minor second peak at $\alpha > 2.5$). Further, the lignin monomer–monomer radial distribution functions (Fig. 4) across temperature space exhibit a single peak (associated with nearest-neighbours along the polymer chain) along with an extended, slowly decaying tail. This long tail and lack of any secondary peaks indicate that the conformations of lignin are open and random within the miscibility gap temperature regime.

An additional benefit from our enhanced sampling is that it allows us to probe the relaxation kinetics from the globule (in pure water) to coil (in THF–water) conformations of lignin. For typical polymer globule-coil transitions at least one intermediate state (a 'molten globule') is traversed.[34] However, when a polymer is in a "poor" solvent with a surfactant present, the intermediate vanishes.[35] This shift to a sharp transition is driven by how "poor" the solvent is for both the surfactant and the polymer, although the extent of this sharpness is also mediated

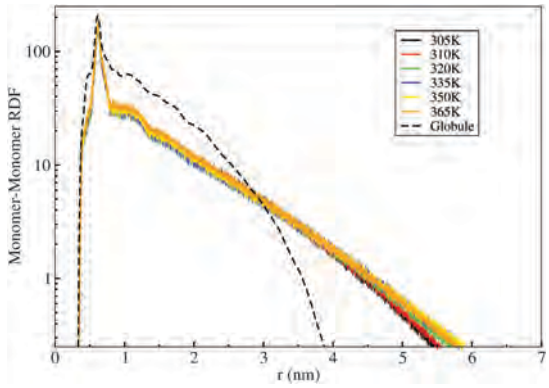


Fig. 4 Radial distribution function of lignin monomers to other monomers in the chain. The first peak corresponds to the nearest neighbouring monomers, while the long tail in the curve indicates a random coil overall structure. The dashed curve corresponds to a globule structure of the same model lignin (61 unit, linear chain). Note that the tail of the distribution has a rapid decline, corresponding to a collapsed state.

by the strength of any favourable surfactant–polymer interaction and the amount of surfactant. In the immiscible regime, THF–water interactions become mildly unfavourable (hence the cloudy/microscopic phase separation) and calculation of the solvent component–lignin interaction energies shows that THF has an interaction energy per molecule with lignin that is 6% more favourable than water with lignin. This, together with the fact that water has been shown to be a poor solvent for lignin,[16,17] allows us to hypothesize that THF acts in a surfactant-like capacity to stabilize the coil state. Using the enhanced sampling provided by our large number of replicas, led to multiple instances (at least 125 times) of lignin "unfolding" from a globule to a coil occurring, which allows us, with proper weighting, to fit these "unfolding" trajectories onto a variety of different kinetic pathways to test the above hypothesis.

As noted above we suspected that THF acts as a surfactant for solubilization of lignin; as such the globule-to-coil transition

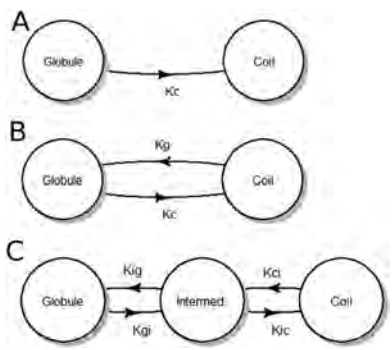


Scheme 1 Kinetic models. (A) "One-state" model, (B) two-state model, (C) three-state (on-pathway intermediate) model.

Table 1 Kinetic constants for "one"-state model evaluated at 298 K

| α cutoff | Kinetic ($K_c$) $(ns)^{-1}$ | $\chi^2$ |
|---|---|---|
| 2.2 | $1.69 \times 10^{-4}$ | $1.90 \times 10^{-1}$ |
| 2.4 | $2.20 \times 10^{-4}$ | $1.84 \times 10^{-1}$ |

 This journal is © the Owner Societies 2016

Published on 26 January 2016. Downloaded by University of Tennessee at Knoxville on 18/08/2016 18:57:32.

Table 2 Kinetic constants and thermodynamics for two-state model evaluated at 298 K

| $\alpha$ cutoff | Kinetic ($K_c$, $K_g$) $(ns)^{-1}$ | | $\Delta G$ (kJ mol$^{-1}$) | $\Delta H$ (kJ mol$^{-1}$) | $T\Delta S$ (kJ mol$^{-1}$) | $\chi^2$ |
|---|---|---|---|---|---|---|
| 2.4 | $3.92 \times 10^{-4}$ | $6.54 \times 10^{-6}$ | −10.19 | −6.89 | 3.33 | $9.04 \times 10^{-2}$ |
| 2.5 | $4.57 \times 10^{-4}$ | $7.99 \times 10^{-6}$ | −10.06 | −4.15 | 5.95 | $8.64 \times 10^{-2}$ |

Table 3 Kinetic constants and thermodynamics for three-state models at 298 K

| $\alpha$ coil | $\alpha$ intr. | Kinetic ($K_{ci}$, $K_{ic}$, $K_{ig}$, $K_{gi}$) $(ns)^{-1}$ | | | | $\Delta G$ (kJ mol$^{-1}$) | $\Delta H$ (kJ mol$^{-1}$) | $T\Delta S$ (kJ mol$^{-1}$) | $\chi^2$ |
|---|---|---|---|---|---|---|---|---|---|
| 2 | 2.2 | $2.53 \times 10^{-4}$ | $4.13 \times 10^{-10}$ | $1.50 \times 10^{-9}$ | $1.98 \times 10^{-5}$ | −33.16 | −33.42 | −0.25 | 1.58 |
| 2.2 | 2.5 | $4.50 \times 10^{-4}$ | $1.70 \times 10^{-10}$ | $1.28 \times 10^{-10}$ | $4.05 \times 10^{-15}$ | −37.25 | −35.36 | 1.89 | 1.43 |

should lack any obvious intermediates, while if the surfactant behaviour is absent the alternate kinetic model would be a three-state model with an on-path intermediate. In addition to the two- and three-state models, as our other structural measures only show a single state, it will be interesting to also consider a "one-state" model, *i.e.*, a model with two states but no return pathway. Scheme 1 below provides a visual summary of the kinetic models tested.

The typical methodology to test these pathways would be to perform a histogram-like (T-WHAM or otherwise[36–38]) free-energy analysis of the simulations and then build possible kinetic pathways from the resulting energy measurements. However, as indicated by our own projections of the energy landscape, only a single dominant extremum is present, indicating a large energy barrier and thus a limitation of equilibrium sampling. An alternative method that allows us to follow the relaxation from one state to another, and is largely invariant to the size of the energy barrier between the states, is to obtain kinetic rate constants by directly fitting the trajectories to the appropriate kinetic rate equations (*i.e.* differential equations that describe the fraction of the system in a particular state at any given time). From these constants the barrier can be evaluated and differences in the goodness-of-fit between models can be used to discriminate between the one-, two-, and three-state kinetic schemes. This alternative methodology is implemented in the tool g_kinetics[39] (see ref. 39 for more details) and is used here with the fractal dimension as our reaction coordinate. The error in this method (noted as $\chi^2$) is quantified by the average squared difference in the average fraction of folded lignin conformations from all of the replicas at a given time and the fit. Thus, the range in the quality of the fit goes from 0 (a perfect fit) to the number of replicas used (in our study 125).

Here, a coil lignin state is defined as having a mass fractal dimension smaller than a given cutoff. Following the suggestion of ref. 39, we performed a number of fits to our data, varying the cutoff value of $\alpha$ to provide a thorough sweep of the kinetic model's parameter space. The results of this sweep are summarized in ESI‡ as Tables S1–S3. The top two best fits for each model (those with the lowest $\chi^2$ values) are presented below in Tables 1–3. The free energy $\Delta G$ for the transition from globule to coil can be obtained at any temperature from the fitted kinetic constants. The slope and $y$-intercept of the resulting $\Delta G$ (not shown) as a function of temperature curve are taken as the $\Delta S$ and $\Delta H$ values, respectively.

From the tables, it is clear that the best fits occur for the two-state model. The globule-to-coil transition is spontaneous at room temperature (as noted by the negative $\Delta G$ at room temperature), and is both enthalphically and entropically favourable (with the entropy being the slightly larger driving factor). It is also interesting that the one-state model *i.e.*, the model with no return from the coil to the globule state, has $\chi^2$ values only slightly worse than those of the two-state model (see ESI‡ tables). This can be explained by the large ($\sim$10 kJ mol$^{-1}$) free-energy difference between the globule and coil states found in the two-state kinetics (highlighted by the presence of a dominant single state in Fig. 2 and ESI‡). In contrast, the best fit for the three-state model has an error value an order of magnitude worse than the fits to either the two- or one-state models, substantiating our observation that there is no intermediate state involved in the globule to coil transition of lignin in the THF–water cosolvent.

## Conclusions

From the present simulations it is clear that, in a THF–water cosolvent system, regardless of being in the miscible or immiscible temperature regimes, lignin is a coil. The domination of the coil state is visible from the distributions of fractal-dimension, whose maximum $\alpha \approx 1.5$ (and indeed the width of distribution in general) is well below the cutoff for a coil state. Also, in this cosolvent system the globule state of lignin transitions directly to a random coil, as is clear from analysis of the possible kinetic pathways of the transition from globule to coil states. The direct transition to a coil supports the hypothesis that THF is surfactant-like for lignin solubilization within the immiscibility gap temperature region. Furthermore, as this effect is invariant to the temperature of the system, the results suggest that CELF may be an effective means to separate lignin from cellulose even at low (non-boiling/pre-immiscibility gap) temperatures.

## Acknowledgements

This work was supported by the BioEnergy Science Center, a U.S. Department of Energy (DOE) Bioenergy Research Center supported by the Office of Biological and Environmental Research in the DOE Office of Science. This research used resources of the Oak Ridge Leadership Computing Facility at the Oak Ridge National Laboratory, which is supported by the

Published on 26 January 2016. Downloaded by University of Tennessee at Knoxville on 18/08/2016 18:57:32.

Office of Science of the U.S. Department of Energy under Contract No. DE-AC05-00OR22725. This research also used the computing resources provided by the U.S. Department of Energy's National Energy Research Scientific Computing Center.

## Notes and references

1 A. D. Sagar and S. Kartha, *Annu. Rev. Environ. Resour.*, 2007, **32**, 131–167.
2 H. Jorgensen, J. B. Kristensen and C. Felby, *Biofuels, Bioprod. Biorefin.*, 2007, **1**, 119–134.
3 S. Contreras, A. R. Gaspar, A. Guerra, L. A. Lucia and D. S. Argyropoulos, *Biomacromolecules*, 2008, **9**, 3362–3369.
4 C. Crestini, F. Melone, M. Sette and R. Saladino, *Biomacromolecules*, 2011, **12**, 3928–3935.
5 S. E. Harton, S. V. Pingali, G. A. Nunnery, D. A. Baker, S. H. Walker, D. C. Muddiman, T. Koga, T. G. Rials, V. S. Urban and P. Langan, *ACS Macro Lett.*, 2012, **1**, 568–573.
6 C. M. Cai, N. Nagane, R. Kumar and C. E. Wyman, *Green Chem.*, 2014, **16**, 3819–3829.
7 C. M. Cai, T. Y. Zhang, R. Kumar and C. E. Wyman, *Green Chem.*, 2013, **15**, 3140–3145.
8 C. M. Cai, T. Y. Zhang, R. Kumar and C. E. Wyman, *J. Chem. Technol. Biotechnol.*, 2014, **89**, 2–10.
9 T. Y. Nguyen, C. M. Cai, R. Kumar and C. E. Wyman, *ChemSusChem*, 2015, **8**, 1716–1725.
10 P. Lejcek, J. Matous, J. P. Novak and J. Pick, *J. Chem. Thermodyn.*, 1975, **7**, 927–935.
11 J. Matous, J. P. Novak and J. Pick, *Collect. Czech. Chem. Commun.*, 1972, **37**, 2653–2663.
12 M. D. Smith, B. Mostofian, X. Cheng, L. Petridis, C. M. Cai, C. E. Wyman and J. C. Smith, *Green Chem.*, 2015, DOI: 10.1039/C5GC01952D.
13 Y. Sugita, A. Kitao and Y. Okamoto, *J. Chem. Phys.*, 2000, **113**, 6042–6051.
14 Y. Sugita and Y. Okamoto, *Chem. Phys. Lett.*, 1999, **314**, 141–151.
15 T. Okabe, M. Kawata, Y. Okamoto and M. Mikami, *Chem. Phys. Lett.*, 2001, **335**, 435–439.
16 L. Petridis, S. V. Pingali, V. Urban, W. T. Heller, H. M. O'Neill, M. Foston, A. Ragauskas and J. C. Smith, *Phys. Rev. E: Stat., Nonlinear, Soft Matter Phys.*, 2011, **84**, 061911.
17 L. Petridis, R. Schulz and J. C. Smith, *J. Am. Chem. Soc.*, 2011, **133**, 20277–20287.
18 L. Petridis and J. C. Smith, *J. Comput. Chem.*, 2009, **30**, 457–467.
19 I. Vorobyov, V. M. Anisimov, S. Greene, R. M. Venable, A. Moser, R. W. Pastor and A. D. MacKerell, *J. Chem. Theory Comput.*, 2007, **3**, 1120–1133.
20 W. L. Jorgensen, J. Chandrasekhar, J. D. Madura, R. W. Impey and M. L. Klein, *J. Chem. Phys.*, 1983, **79**, 926–935.
21 H. J. C. Berendsen, J. P. M. Postma, W. F. Vangunsteren, A. Dinola and J. R. Haak, *J. Chem. Phys.*, 1984, **81**, 3684–3690.
22 G. Bussi, D. Donadio and M. Parrinello, *J. Chem. Phys.*, 2007, **126**, 014101.
23 M. Parrinello and A. Rahman, *J. Appl. Phys.*, 1981, **52**, 7182–7190.
24 B. Hess, H. Bekker, H. J. C. Berendsen and J. G. E. M. Fraaije, *J. Comput. Chem.*, 1997, **18**, 1463–1472.
25 B. Hess, *J. Chem. Theory Comput.*, 2008, **4**, 116–122.
26 S. Miyamoto and P. A. Kollman, *J. Comput. Chem.*, 1992, **13**, 952–962.
27 M. J. Abraham and J. E. Gready, *J. Comput. Chem.*, 2011, **32**, 2031–2040.
28 H. J. C. Berendsen, D. Vanderspoel and R. Vandrunen, *Comput. Phys. Commun.*, 1995, **91**, 43–56.
29 B. Hess, C. Kutzner, D. van der Spoel and E. Lindahl, *J. Chem. Theory Comput.*, 2008, **4**, 435–447.
30 S. Pronk, S. Pall, R. Schulz, P. Larsson, P. Bjelkmar, R. Apostolov, M. R. Shirts, J. C. Smith, P. M. Kasson, D. van der Spoel, B. Hess and E. Lindahl, *Bioinformatics*, 2013, **29**, 845–854.
31 D. Van der Spoel, E. Lindahl, B. Hess, G. Groenhof, A. E. Mark and H. J. C. Berendsen, *J. Comput. Chem.*, 2005, **26**, 1701–1718.
32 L. Hong and J. Z. Lei, *J. Polym. Sci., Part B: Polym. Phys.*, 2009, **47**, 207–214.
33 W. Humphrey, A. Dalke and K. Schulten, *J. Mol. Graphics Modell.*, 1996, **14**, 33–38.
34 C. Wu and X. H. Wang, *Phys. Rev. Lett.*, 1998, **80**, 4092–4094.
35 V. A. Baulin, E. Y. Kramarenko and A. R. Khokhlov, *Comput. Theor. Polym. Sci.*, 2000, **10**, 165–175.
36 E. Gallicchio, M. Andrec, A. K. Felts and R. M. Levy, *J. Phys. Chem. B*, 2005, **109**, 6722–6731.
37 J. D. Chodera, W. C. Swope, J. W. Pitera, C. Seok and K. A. Dill, *J. Chem. Theory Comput.*, 2007, **3**, 26–41.
38 Z. Q. Tan, E. Gallicchio, M. Lapelosa and R. M. Levy, *J. Chem. Phys.*, 2012, **136**, 144102.
39 D. van der Spoel and M. M. Seibert, *Phys. Rev. Lett.*, 2006, **96**, 238102.

 This journal is © the Owner Societies 2016